Springer

Journal of Mechanical Science and Technology 23 (2009) 1517~1527

Journal of Mechanical Science and Technology

www.springerlink.com/content/1738-494x
DOI 10.1007/s12206-009-0406-4

Natural convection heat transfer estimation from a longitudinally finned vertical pipe using CFD †

Hyo Min Jeong[1], Yong Hun Lee[2], Myoung Kuk Ji[2], Kang Youl Bae[3] and Han Shik Chung[1,*]

[1]*Department of Mechanical and Precision Engineering, The Institute of Marine Industry, Gyeongsang National University, 445 Inpyeong-Dong, Tong-yeong, Gyeongsang-namdo, 650-160, Korea*

[2]*Department of Mechanical and Precision Engineering, Gyeongsang National University, 445 Inpyeong-dong,Tongyeong, Gyeongsang-namdo, 650-160, Korea*

[3]*Machine Industry Tech Center, Gyeongnam Technopark, 445 Inpyeong-dong, Tong-young Gyeongsang-namdo, 650-160, Korea*

(Manuscript Received July 24, 2007; Revised February 28, 2009; Accepted March 17, 2009)

Abstract

In this study, CFD analysis of air-heating vaporizers was conducted. A longitudinally finned vertical pipe was used to represent the air-heating vaporizer in the CFD model. Nitrogen gas was used as the working fluid inside the vertical pipe, and it was made to flow upward. Ambient air, which was the heat source, was assumed to contain no water vapor. To validate the CFD results, the convective heat transfer coefficients inside the pipe, $h_{i\text{-}c}$, derived from the CFD results were first compared with the heat transfer coefficients inside the pipe, $h_{i\text{-}p}$, which were derived from the Perkins correlation. Second, the convection heat transfer coefficients outside the pipe, $h_{o\text{-}c}$, derived from the CFD results were compared with the convection heat transfer coefficients, $h_{o\text{-}a}$, which were derived from an analytical solution of the energy equation. Third, the CFD results of both the ambient-air flow pattern and temperature were observed to determine whether they were their reasonability. It was found that all validations showed good results. Subsequently, the heat transfer coefficients for natural convection outside the pipe, $h_{o\text{-}c}$, were used to determine the Nusselt number outside the pipe, $Nu_{o.}$. This was then correlated with the Rayleigh number, R_a. The results show that R_a and Nu_o have a proportional relationship in the range of $2.7414 \times 10^{12} \leq Ra \leq 2.8263 \times 10^{13}$. Based on this result, a relation for the Nusselt number outside the pipe, Nu_o, was proposed.

Keywords: CFD; Natural convection; Heat transfer; Vertical pipe; Fin

1. Introduction

To allow liquefied natural gas (LNG) to return to its gaseous state, LNG is typically fed into a regasification plant, in which LNG is vaporized using a heat exchanger called a "vaporizer." An air-heating vaporizer is normally used at the inland/satellite receiving terminal for such purposes. However, this type of vaporizer has a constraint: it has small-to-medium production capacity due to the small heat capacity of air used as its heat source [1].

Therefore, to meet the increasing demand for LNGs in inland areas (where pipelines do not exist or are difficult to construct), some studies aiming to develop the best-performing air-heating vaporizers are currently underway.

Computational Fluid Dynamics is considered a powerful and an almost essential tool for the design, development, and optimization of engineering applications. [2] investigated the effect of fin quantity, fin thickness, and fin length for the heat transfer rate of longitudinally finned air-heating vaporizers using 2D numerical analysis. [3] and [4] conducted 2D numerical analysis to determine the optimum dimensions of

† This paper was recommended for publication in revised form by Associate Editor Man Yeong Ha

*Corresponding author. Tel.: +055 640 3185, Fax.: +055 640 3188
E-mail address: hschung@gnu.ac.kr

longitudinally finned air-heating vaporizers. They proposed a 4-fin type of vaporizer with a fin thickness of 2 mm as the optimum dimension. [5] numerically analyzed the laminar free convection around a horizontal cylinder having longitudinal fins of finite thickness.

A vaporizer is actually a heat exchanger. Many studies on heat exchangers have been conducted in the past. One of the main problems in heat exchangers, however, has been frost formation due to the condensation and freezing of the water vapor present in air. These ice deposits lead to a decreased heat transfer rate because the thermal conductivity of ice is less than one-fortieth of that of aluminum alloy.

In general, heat transfer efficiency is less for thicker ice. In addition, when fins are covered with thick ice (in the case of vaporizers such as finned type vaporizers), the effective heat transfer area decreases until their configuration becomes almost invisible [6]. [7] conducted experiments to determine the effects of various factors (fin pitch, fin arrangement, air temperature, air humidity, and air velocity) on the frost growth and thermal performance of a fin-tube heat exchanger. General solutions for the optimum dimensions of convective longitudinal fins with base-wall thermal resistance capacities were solved analytically by [8]. Meanwhile, [9] conducted studies to determine the optimal values of the design parameters for a fin-tube heat exchanger in a household refrigerator under frosting conditions. [10-11] conducted both numerical and experimental studies on the frost formation in fin-and-tube heat exchangers.

It is well known that an LNG vaporizer consists of a vaporizing section and a heating section. In this study, we focused on the heating section of a vaporizer in which there is no phase change in the working fluid inside (i.e., the fluid remains in the gas phase). Aiming to determine the correlation of the Nusselts number for natural convection occurring outside the vaporizer, a 3D CFD analysis of a longitudinally finned air-heating vaporizer (represented by a longitudinally finned vertical pipe) with 4 fins, a fin length of 75 mm, and a fin thickness of 2 mm (denoted by 4fin75le) was conducted. The correlation equation between the Nusselt number outside the pipe and the Rayleigh number (Ra) is given in the form of Eq. (1):

$$Nu_o = C(Ra)^m . \quad (1)$$

The vaporizers were chosen to be 4-fin type on the basis of a 2D numerical analysis conducted by Jeong *et al.* (2006); they concluded that the optimum vaporizer geometry is a vaporizer with an angle of 90^o between fins and a fin thickness of 2 mm. This implies that the vaporizer should have 4 longitudinal fins. They asserted that this is because such vaporizers would have an optimum heat transfer rate taking into consideration the presence of frost deposit (Jeong *et al.*, 2006).

2. Numerical simulation

Fig. 1 and Fig. 2 show the 3D mesh model used for CFD analysis, while

Fig. 3 shows the dimensions of the basic model. The mesh was constructed using a commercial software, Star-CD, which was built by the CD adapco Group. The cell quantity amounted to 272,892 cells. The model consists of ambient air as the heat source, a finned vertical pipe whose length is 1000 mm, and nitrogen gas flowing upward inside the pipe. Given that there is heat transfer from the fluid to the solid phase, the Star-CD conjugate heat transfer mode was used. The length and thickness of the fins were 75 mm (from the outer surface of the pipe) and 2 mm, respectively. The inner and outer diameters of the pipe were 24 mm and 30 mm, respectively. The mesh model created was made one-fourth of the real model in order to accelerate the iteration.

Natural convection refers to the heat transfer that occurs between ambient air and the finned vertical pipe . After calculating the predictions of the Grashof number for natural convection along a 1000 mm vertical pipe (under the assumption that the average outer surface temperature of the pipe was the same as the nitrogen inlet temperature), it was expected that the downward flow of ambient air as caused by the cooling effect was turbulent flow ($Gr > 10^9$), [12]. Hence, a k-omega-SST-turbulent low Reynolds number model was used as the turbulence model. It is more accurate in predicting phenomena in such cases as when turbulent natural convection or buoyancy forces play a major role in driving the flow. The K-omega-SST model applies a combination of the k-omega model equations implemented near the wall region; the k-epsilon turbulence model must be employed in the bulk or free flow region [13, 14].

The mesh of ambient air near the pipe was made finer so that the results for a low Reynolds model could be more accurate; the dimensions were 0.6–6 mm measured from the wall. Moreover, the " hybrid

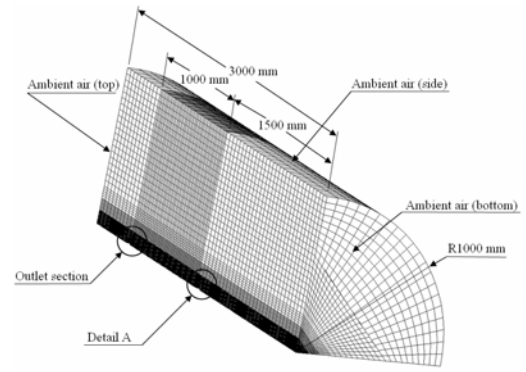

(a) Whole mesh model

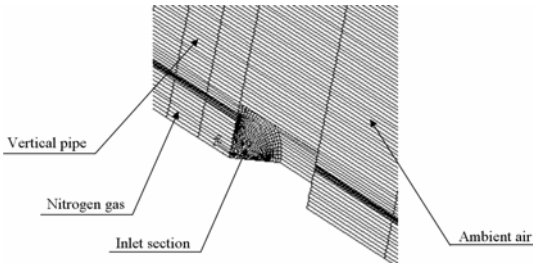

(b) Detail A

Fig. 1. Figure of the whole mesh model and the detailed view of the inlet section.

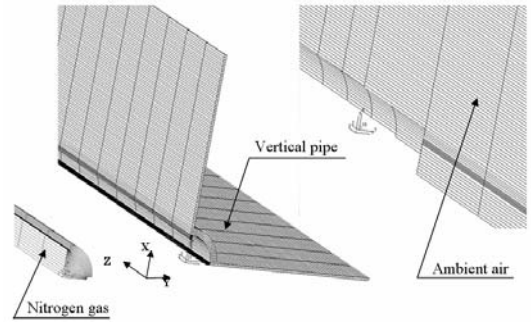

Fig. 2. Explode figure of the 3D model.

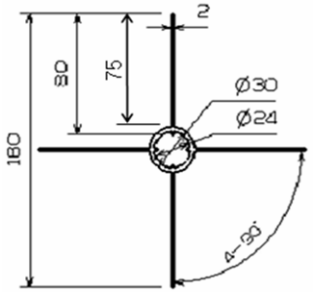

Fig. 3. Cross-sectional drawing of the finned vertical pipe.

wall" boundary condition was chosen for the near-wall ambient air so that we need not ensure a sufficiently small near-wall value for y^+ (by creating a sufficiently fine mesh next to the wall). Such hybrid wall boundary condition provides valid boundary conditions for momentum, turbulence, energy, and species variables for a wide range of near-wall mesh densities [15].

The PISO algorithm was used to solve pressure terms because the calculation of natural convection problems could be easier using this algorithm. The differencing schemes used were the Monotone Advection and Reconstruction Scheme (MARS) for momentum, temperature, and density calculations, and the up-wind scheme for turbulence kinetic energy, as well as turbulence dissipation rate calculations.

The boundary conditions used for ambient air far from the pipe (side ambient air) were "wall" under slip conditions and a temperature of 293 K (temperature of the ambient air). "Symmetry"" boundary conditions were applied at the top and bottom areas of the ambient air model. In this numerical analysis, the buoyancy effect on the temperature profile has been neglected because a conjugate model was applied in this analysis to calculate the body (pipe) parameters (see Fig. 2 and Fig. 3). The boundary condition of the solid-fluid interface was automatically set to "conducting no-slip wall" whenever the conjugate heat transfer mode was used. In this CFD analysis, ambient air was assumed to contain no water vapor (dry air) since it was focused on the basic heat transfer characteristics of the pipe. The air properties other than density were constant. The density changed only with temperature and followed the ideal gas law. The thermal conductivity of the pipe (pure aluminum) was set to 269.5 W/mK or 237 W/mK, depending on whether the average pipe temperature was predicted as approximately 150 K or 200 K, respectively.

The flow inside the pipe was assumed to be fully developed. At the pipe inlet, the "pressure" boundary condition was used with the pressure maintained constant at 2 bar absolute, while the inlet temperature was varied.

Furthermore, at the inlet, the turbulence length scale value was based on 7% of the hydraulic diameter, and the turbulence intensity was based on the following equation:

$$I = 0.16\,\mathrm{Re}^{-\frac{1}{8}}. \quad (2)$$

Table 1. The conditions used for the simulation.

No	flow rate (kg/s)	Tb inlet (K)	T ambient (K)	Inlet pressure (bar)
1	0.015	111	293	2
2	0.020	111		
3	0.030	100		
4	0.015	131		
5	0.010	131		
6	0.005	151		
7	0.010	151		
8	0.005	171		
9	0.010	171		
10	0.005	191		
11	0.010	191		
12	0.005	211		
13	0.010	211		
14	0.005	231		
15	0.010	231		
16	0.025	111		
17	0.030	111		
18	0.020	131		
19	0.025	131		
20	0.015	151		
21	0.020	151		
22	0.015	171		
23	0.020	171		
24	0.025	151		

The pipe outlet boundary condition was "outlet" with the mass flow rate set at various values.

The turbulence model used for the nitrogen flowing inside was a k-epsilon high Reynolds number because the flow was fully turbulent (R e> 10^4). The steady state simulation was conducted under 24 different conditions as listed in Table 1.

3. Calculations and validation

The CFD results were used to calculate the convective heat transfer coefficient inside the pipe, $h_{i\text{-}c}$, and outside the pipe, $h_{o\text{-}c}$, using the following equations:

$$\dot{m}\left(i_{out}-i_{in}\right)=h_{i-c}A_{si}\left(T_{si}-T_{bi}\right) \quad \text{and} \tag{3}$$

$$\dot{m}\left(i_{out}-i_{in}\right)=h_{o-c}A_{so-all}\left(T_{\infty}-T_{so-all}\right). \tag{4}$$

The enthalpy data were taken from NIST [16] with ASHRAE Standard State Convention.

To validate the CFD results, first, the convection

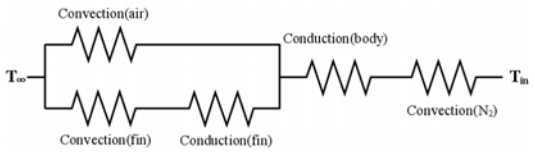

Fig. 4. Thermal circuit at the outer side of the pipe.

heat transfer coefficients inside the pipe, $h_{i\text{-}c}$ which were calculated using Eq. (3) were compared with the convection heat transfer coefficients, $h_{i\text{-}p}$, which were derived from the Perkins and Worsoe-Schmidt correlation [17], along with Nusselt number definition.

The Perkins correlation is as follows:

$$Nu_{i-p}=0.024\,Re_{b-in}^{0.8}\,Pr_{b-in}^{0.4}\left(\frac{T_{si}}{T_{b-in}}\right)^{-0.7}\left[1+\left(\frac{\ell}{d_i}\right)^{-0.7}\left(\frac{T_{si}}{T_{b-in}}\right)^{0.7}\right], \tag{5}$$

while the Nusselt number definition is as follows:

$$Nu_{i-p}=\frac{h_{i-p}\,d_i}{k_{N_2}}. \tag{6}$$

All data used were taken from the input data and CFD results, after which the convection heat transfer coefficient, $h_{i\text{-}p}$, was determined. Second, the convection heat transfer coefficients outside the pipe, $h_{o\text{-}c}$, that were calculated using Eq. (4) were compared with the convection heat transfer coefficients, $h_{o\text{-}a}$, which were derived using an analytical solution of the energy equation. These convection heat transfer coefficients outside the pipe, $h_{o\text{-}a}$, were calculated by simultaneously solving Eqs. (7)-(14) given below. The value of $h_{o\text{-}a}$ was obtained by substituting the data from the experimental results in the energy equation. These equations were analytically derived from the energy equation [18].

Fig. 4 shows the thermal circuit of the outer side of the pipe; it also illustrates the heat transfer from the pipe to ambient air. This coefficient, $h_{o\text{-}a,}$ was assumed to be homogenous across the outer side of the pipe.

$$\dot{Q}=\frac{T_{\infty}-T_{so}}{R_e}; \tag{7}$$

where

$$R_e=\left(\frac{1}{R_b}+\frac{1}{R_{f\,all\,fins}}\right)^{-1}; \tag{8}$$

$$R_b = \frac{1}{h_{o-a}(2\pi r_o - nt)\ell}; \quad (9)$$

$$R_{f\ one\ fin} = \frac{T_\infty - T_{so}}{\dot{Q}_f} = \frac{\cosh(mL) + (h_o/mk_{al})\sinh(mL)}{(h_{o-a}Pk_{al}A_c)^{1/2}(\sinh(mL) + (h_o/mk_{al})\cosh(mL))}; \quad (10)$$

$$m = \left(\frac{h_{o-a}P}{k_{al}A_c}\right)^{1/2}; \quad (11)$$

$$P = 2(\ell + t); \quad (12)$$

$$A_c = \ell \times t; \quad (13)$$

$$R_{f\ all\ fins} = \frac{T_\infty - T_{so}}{n\dot{Q}_f}; \quad (14)$$

Given that all values above are known (from the input data and CFD results) with the exception of h_{o-a}, the convection heat transfer coefficients outside the pipe, $h_{o-a,}$ can thus be calculated. Third, to ensure the validity of the CFD results, the ambient air flow pattern and temperature were observed to determine their reasonability.

Next, after validation, the Nusselt numbers outside the pipe, $Nu_{o,}$ were calculated using:

$$Nu_o = \frac{h_{o-c}\ell_c}{k_\infty} \quad . \quad (15)$$

These Nusselt numbers outside the pipe Nusselt numbers, Nu_o, were correlated with the Rayleigh numbers, Ra, which were in turn determined using:

$$Ra = \frac{g\beta(T_\infty - T_{so-all})\ell_c^{\,3}}{\nu\alpha} \quad \text{and} \quad (16)$$

$$\beta = 1/T_f \ ; \quad T_f = \frac{T_{so-all} + T_\infty}{2} \quad . \quad (17)$$

The characteristic length, ℓ_c used for calculating Nu_o and Ra is defined as follows:

$$\ell_c = \frac{\left[\pi d_o - nt + (2\times L + t)\times n\right]\times \ell}{\pi d_o}. \quad (18)$$

This characteristic length was used to consider the fin length and thickness under the assumption that the fin thickness was so small that the base surface covered by the fin is almost a flat plane.

4. Results and discussions

The heat transfer coefficients, $h_{i-c,}$ of the inner pipe, which were calculated using the CFD results, showed a good agreement with the heat transfer coefficients, $h_{i-p,}$ of the inner pipe, which were determined through the Perkins' correlation, as shown in Table 2. It is considered that the Perkins Nusselt correlation has limitations in the ratio of surface temperature to inlet bulk temperature (T_{si}/T_{b-in}) $1.24 < T_{si}/T_{b-in} < 7.54$.

From the value of "T_{si}/T_{b-in}"in Table 2 (marked by an asterisk), it can be seen that there are only 12 data sets that meet the requirement of the Perkins correlation, provided that the limit is considered to be one digit after the decimal point, that is, $1.2 < T_{si}/T_{b-in} < 7.5$. Nevertheless, these 12 data sets sufficiently demonstrated that the 3D model was valid for simulation, implying that the other CFD simulation results were valid. The second validation, that is, the comparison of h_{o-a} to h_{o-c}, showed good results. Their discrepancy was within 4%, as shown in Table 2.

The results of these two validations imply that the CFD results of heat transfer were valid. Table 2 also shows that for constant temperature, the increase in mass flow rate leads to a significant increase in the convection heat transfer coefficient inside the pipe.

The above results only validate the results of CFD on heat transfer. Therefore, as the third step, and to ensure that the CFD results outside the pipe are also valid (i.e., actual natural convection), the flow pattern of ambient air and its temperature were observed. Due to the fact that the phenomena for ambient air were logically acceptable, it can be concluded that the CFD results were quite promising in predicting the natural convection heat transfer outside the pipe. The relevant explanations are as follows.

From Fig. 5, Fig. 6, and Fig. 7, it can be seen that ambient air flowed downward with increasing velocity. This is because the low temperature of the wall decreases the temperature of ambient air such that the density of air near the wall increases, while the density of ambient air sufficiently far from the pipe does not. Moreover, the upward flow of nitrogen causes the wall temperature on the upstream to be lower than that on the downstream. This condition results in the constantly increasing density of the near-wall ambient air as it flows downward. The fluid velocity near the wall is zero because of the no-slip condition; the velocity then continues to increase as the distance from the wall increases until it reaches a maximum. How-

Table 2. Comparison of $h_{i\text{-}c}$ to $h_{i\text{-}p}$ and $h_{o\text{-}c}$ to $h_{o\text{-}a}$.

No	Mass flow rate (kg/s)	$T_{b\text{-}in}$ (K)	$h_{i\text{-}c}$	$h_{i\text{-}p}$	Discrepancy between $h_{i\text{-}c}$ and $h_{i\text{-}p}$ (%)	$T_{si}/T_{b\text{-}in}$	$h_{o\text{-}c}$	$h_{o\text{-}a}$	Discrepancy between $h_{o\text{-}c}$ and $h_{o\text{-}a}$ (%)
1	0.0150	111	91.00	89.41	2 (+)	1.34*	2.26	2.18	4 (+)
2	0.0200	111	117.30	115.16	2 (+)	1.30*	2.44	2.36	4 (+)
3	0.0300	100	166.10	155.44	7 (+)	1.31*	3.00	2.90	3 (+)
4	0.0150	131	93.30	96.72	4 (-)	1.24*	3.83	3.72	3 (+)
5	0.0100	131	65.40	67.84	4 (-)	1.30*	2.14	2.07	4 (+)
6	0.0050	151	37.20	39.71	6 (-)	1.32*	1.97	1.91	4 (+)
7	0.0100	151	67.80	72.70	7 (-)	1.22*	1.69	1.63	4 (+)
8	0.0050	171	38.10	42.41	10 (-)	1.23*	1.87	1.80	4 (+)
9	0.0100	171	69.40	76.73	10 (-)	1.16	1.58	1.53	4 (+)
10	0.005	191	39.70	44.80	11 (-)	1.16	1.77	1.71	3 (+)
11	0.010	191	73.50	80.20	8 (-)	1.11	1.48	1.43	3 (+)
12	0.005	211	40.20	46.83	14 (-)	1.11	1.71	1.66	3 (+)
13	0.010	211	76.10	83.07	8 (-)	1.08	1.37	1.33	3 (+)
14	0.005	231	42.00	48.63	14 (-)	1.07	1.68	1.63	3 (+)
15	0.010	231	80.70	85.55	6 (-)	1.05	1.27	1.24	3 (+)
16	0.025	111	154.90	140.95	10 (+)	1.25*	1.73	1.68	3 (+)
17	0.030	111	188.10	164.40	14 (+)	1.23*	1.17	1.14	3 (+)
18	0.020	131	121.10	123.63	2 (-)	1.22*	1.92	1.88	3 (+)
19	0.025	131	149.50	148.76	1 (+)	1.20*	2.60	2.51	3 (+)
20	0.015	151	98.90	102.85	4 (-)	1.18	2.92	2.83	4 (+)
21	0.020	151	132.60	130.80	1 (+)	1.16	2.39	2.32	4 (+)
22	0.015	171	103.40	107.74	4 (-)	1.13	2.76	2.68	4 (+)
23	0.020	171	141.40	136.30	4 (+)	1.12	2.09	2.02	3 (+)
24	0.025	151	170.40	156.85	9 (+)	1.15	2.45	2.37	3 (+)

* Simulations that meet the Perkins-correlation requirement of $1.2 < T_{si}/T_{b\text{-}in} < 7.5$

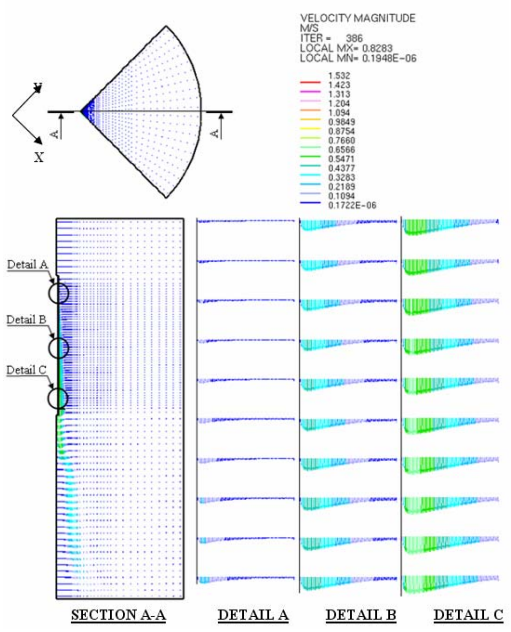

Fig. 5. Flow pattern of ambient air for the simulation condition of inlet temperature and mass flow rate 231 K and Re = 3.5367E+4, respectively. Ra = 2.7414E+12.

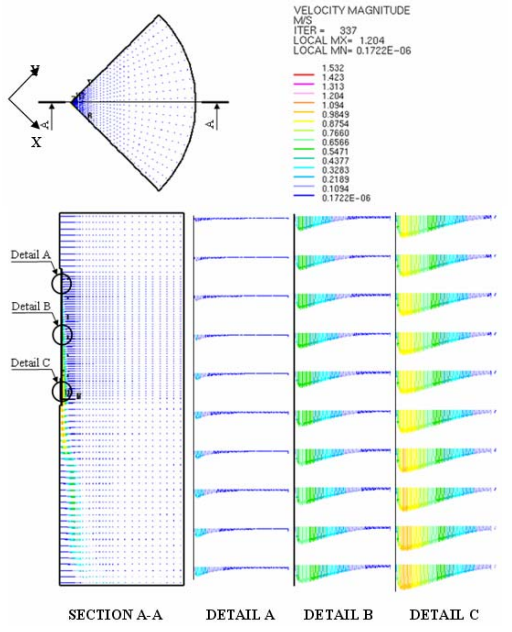

Fig. 6. Flow pattern of ambient air for the simulation condition of inlet temperature and mass flow rate 171 K and Re = 6.9342E+4, respectively. Ra = 9.4131E+12.

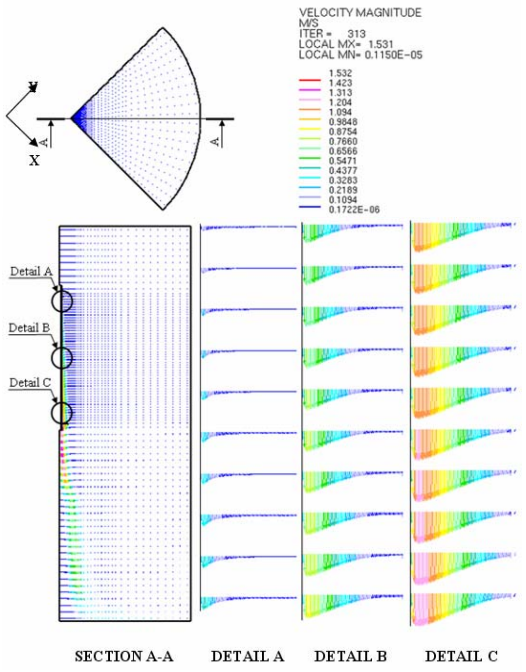

Fig. 7. Flow pattern of ambient air for the simulation condition of inlet temperature and mass flow rate 100 K and Re = 1.07276E+5, respectively. Ra = 2.8263E+13.

ever, when the distance from the wall increases, the velocity begins decreasing until it reaches zero due to the decrease in density difference. This velocity profile is also influenced by the viscosity of the fluid. The ambient air far from the pipe is quiescent.

Fig. 9 (refer to detail A of Fig. 8 to read this figure) shows a comparison of the turbulence kinetic energy of the flow between three simulations with an increasing Rayleigh number, that is, it illustrates a comparison between the lowest, middle, and highest Ra results from the simulations. In all simulations, the flow is turbulent. The turbulence intensity increases when the Rayleigh number increases. As shown in Fig. 9, there are significant temperature differences between the wall and air. This may be due to the higher Rayleigh number brought about by the increasing temperature difference between the atmosphere and the external wall of the pipe.

Fig. 10 (refer to detail A of Fig. 8 to read this figure) illustrates the temperature of ambient air with three different simulations. The temperature on the lower side of the pipe was lower than that on the upper side because of the upward flow of nitrogen inside the pipe. All these phenomena show that the CFD results represent turbulent natural convection.

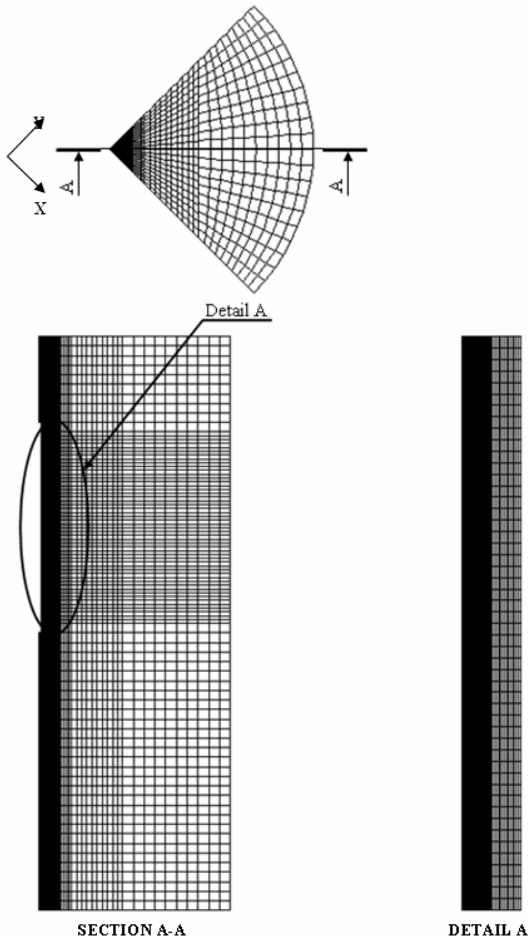

Fig. 8. Drawing view which is used for Fig. 9 and Fig. 10.

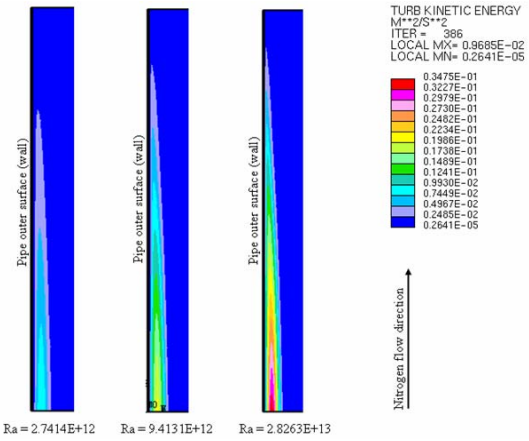

Fig. 9. Figures of ambient air beside the pipe (excluding the ambient air on the top and the bottom of the pipe). This illustrates the turbulence kinetic energy of near-wall ambient air.

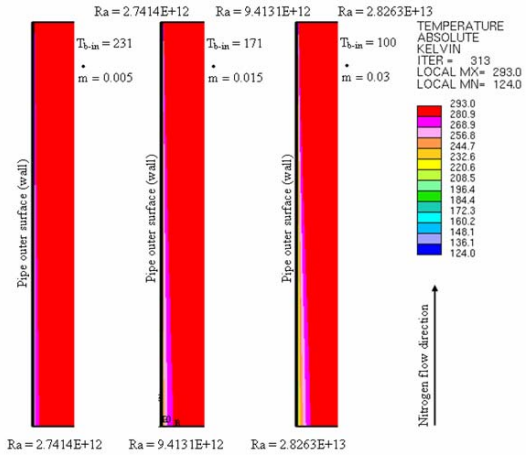

Fig. 10. Figures of ambient air beside the pipe (excluding the ambient air on the top and the bottom of the pipe). This illustrates the temperature of near-wall ambient air.

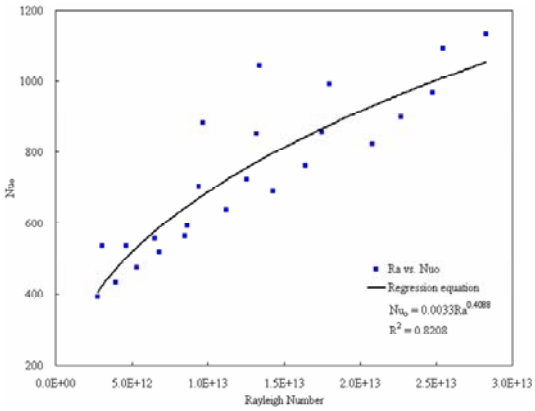

Fig. 11. Graph of Nusselt numbers outside the pipe vs. the Rayleigh numbers.

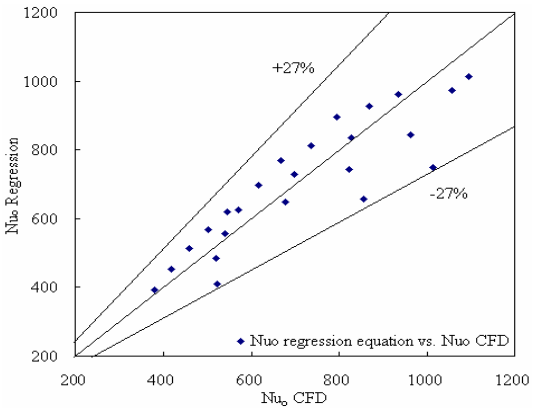

Fig. 12. Nusselt numbers outside the pipe derived from the regression equation vs. the Nusselt numbers outside the pipe of the original CFD results.

Next, after this validation, the outer-pipe Nusselt numbers were determined using Eq. (15). These were then correlated with the Rayleigh number calculated using Eq. (16). The results are shown in Table 3 and Fig. 11. This table has been sorted by ascending Rayleigh numbers. From the table and figure, it can be concluded that Nu_o is proportional to Ra over the range of $2.7414 \times 10^{12} \le Ra \le 2.8263 \times 10^{13}$; the regression equation is as follows:

$$Nu_o = (0.0033)\, Ra^{0.4088} \quad , \tag{19}$$

and the correlation coefficient is $R^2 = 0.8208$.

In this case, the multiple correlation coefficients, R, and the coefficient of determination, R^2, are both measures of how well the regression model describes the data. R values near 1 indicate that the equation is a good description of the relation between the independent and dependent variables. R equals 0 when the values of the independent variable do not allow any prediction of the dependent variables, and it equals 1 when the dependent variables can be predicted perfectly from the independent variables. This regression equation has uncertainty within 27%, as shown in Table 3 and Fig. 12. Additional simulations should be conducted to obtain more accurate Nu_o correlations over a wider Ra range.

5. Conclusions

Here, CFD analysis was conducted on a 1000 mm long, longitudinally finned vertical pipe with 4 fins, a fin length of 75 mm, and a fin thickness of 2 mm in which nitrogen gas was made to flow; the pipe was heated by using static dry-ambient air outside the pipe. Therefore, the conditions under which these simulations were performed were non-uniform wall heat flux and non-uniform wall temperature conditions. The objective was to obtain natural convection correlation outside the pipe. The correlation equation proposed is as follows:

$$Nu_o = (0.0033)\, Ra^{0.4088}$$

for the Rayleigh number in the range of $2.7414 \times 10^{12} \le Ra \le 2.8263 \times 10^{13}$; the uncertainty was equal to 27% with the correlation coefficient

$$R^2 = 0.8208$$

Table 3. Calculated Rayleigh numbers and the Nusselt numbers outside the pipe.

No	Mass flow rate (kg/s)	$T_{b\text{-}in}$ (K)	Ra ambient air	Nu_o CFD	Nu_o regression	Discrepency (%)
1	0.005	231	2.7414E+12	391.528	401.012	2 (+)
2	0.010	231	3.0697E+12	534.433	419.990	21 (-)
3	0.005	211	3.9165E+12	431.856	463.971	7 (+)
4	0.010	211	4.6059E+12	535.139	495.766	7 (-)
5	0.005	191	5.2944E+12	473.843	524.820	11 (+)
6	0.010	191	6.4691E+12	557.623	569.622	2 (+)
7	0.005	171	6.7748E+12	518.085	580.476	12 (+)
8	0.005	151	8.4583E+12	563.191	635.605	13 (+)
9	0.010	171	8.6274E+12	590.722	640.769	8 (+)
10	0.015	171	9.4131E+12	703.418	664.012	6 (-)
11	0.020	171	9.6818E+12	882.479	671.696	24 (-)
12	0.010	151	1.1201E+13	638.121	712.935	12 (+)
13	0.015	151	1.2547E+13	723.740	746.788	3 (+)
14	0.020	151	1.3188E+13	851.205	762.155	10 (-)
15	0.025	151	1.3384E+13	1043.895	766.765	27 (-)
16	0.010	131	1.4262E+13	690.870	786.942	14 (+)
17	0.015	131	1.6360E+13	762.283	832.355	9 (+)
18	0.020	131	1.7479E+13	856.698	855.174	0 (-)
19	0.025	131	1.7965E+13	991.500	864.816	13 (-)
20	0.015	111	2.0787E+13	824.090	917.967	11 (+)
21	0.020	111	2.2695E+13	899.121	951.521	6 (+)
22	0.025	111	2.4734E+13	967.440	985.582	2 (+)
23	0.030	111	2.5444E+13	1091.474	997.051	9 (-)
24	0.030	100	2.8263E+13	1133.577	1040.811	8 (-)

Additional numerical analysis should be conducted to obtain a more accurate correlation for the Nusselt number over a wider Rayleigh number range. Moreover, this correlation equation must be validated by an experiment.

Acknowledgement

The authors are grateful for the support provided by the Brain Korea 21 Project, the Ministry of Commerce, Industry, and Energy (MOCIE), and the Korea Industrial Technology Foundation (KOTEF) through the Human Resource Training Project for Regional Innovation.

Nomenclature

A_c : Fin cross-sectional area, m^2
A_{si} : Inside pipe surface area, m^2
$A_{so\text{-}all}$: Outside pipe surface area (including the fins), m^2
d_i : Inside diameter of the pipe, m
d_o : Outside diameter of the pipe, m
g : Gravitational acceleration, m/s^2
Gr_x : Local Grashof number
$h_{i\text{-}c}$: Average heat transfer coefficient inside the pipe derived from the CFD results, W/m^2K
$h_{i\text{-}p}$: Average heat transfer coefficient inside the pipe derived from the Perkins correlation, W/m^2K
$h_{o\text{-}c}$: Average heat transfer coefficient outside the pipe derived from the CFD results, W/m^2K
$h_{o\text{-}a}$: Average heat transfer coefficient outside the pipe derived from the analytical solution of the energy equation, W/m^2K
i_{in} : Enthalpy at pipe inlet, Joule/kg
i_{out} : Enthalpy at pipe outlet, Joule/kg
k_{al} : Thermal conductivity of aluminum, W/mK
k_{N2} : Thermal conductivity of nitrogen, W/mK
k_∞ : Thermal conductivity of ambient air, W/mK
L : Fin length (radial direction), m

ℓ : Length of the pipe, m
ℓ_c : Characteristic length of the pipe, m
$\dot{m}$: Mass flow rate, kg/s
n : Number of fin
Nu_{i-p} : Nusselt number inside the pipe calculated using Perkins correlation
Nu_o : Nusselt number outside the pipe
Pr : Prandtl number
$\dot{Q}$: Total heat transfer rate, W
$\dot{Q}_f$: Heat transfer rate from the fin, W
R : Multiple correlation coefficient
R^2 : Coefficient of determination
Ra : Rayleigh number
Re : Reynolds number
R_b : Pipe base thermal resistance, K/W
R_e : Equivalent thermal resistance, K/W
R_f : Fin thermal resistance, K/W
t : Fin thickness, m
T_{bi} : Fluid mean bulk temperature inside the pipe, K
T_{b-in} : Fluid bulk temperature at the inlet of the pipe, K
T_f : Film temperature, K
T_{si} : Pipe inner surface mean temperature, K
T_{so} : Pipe outer surface mean temperature (excluding the fin temperature), K
T_{so-all} : Pipe outer surface mean temperature (base and fin temperature), K
T_∞ : Ambient temperature, K
α : Thermal diffusivity, m^2/s
β : Coefficient of thermal expansion, K^{-1}
ν : Kinematic viscosity, m^2/s

References

[1] K. Sugano, Aug. LNG Vaporizers, *Research and Development, Kobe Steel Engineering Reports,* 56, No. 2 (2006).

[2] S. C. Lee, Y. H. Lee, H. S. Chung, H. M. Jeong, C. K. Lee and Y. H. Park, Effects on Heat Transfer of Super Low Temperature Vaporizer Respect with of Geometric Parameters, *2nd International Conference on Cooling and Heating Technologies,* Dalian, China, July 26 – 30 (2006).

[3] H. M. Jeong, H. S. Chung, S. C. Lee, T. W. Kong and C. S. Yi, Optimum Design of Vaporizer Fin with Liquefied Natural Gas by Numerical Analysis, *Journal of Mechanical Science and Technology (KSME Int. J.),* 20, No. 4, (2006) 545-553.

[4] T. W. Kong, S. C. Lee, Y. H. Lee, H. S. Chung and H. M. Jeong, A Study on The Air Vaporizer for Liquefied Natural Gas with Super Low Temperature, *Proceedings of the 3rd Asian Conference on Refrigeration and Air-conditioning,* May 21-23, Gyeongju, South Korea (2006).

[5] S. C. Haldar, G. S. Kochhar, K. Manohar and R. K. Sahoo, Numerical Study of Laminar Free Convection about A Horizontal Cylinder with Longitudinal Fins of Finite Thickness, *International Journal of Thermal Sciences, article in press* (2006).

[6] N. Morimoto, S. Yamamoto, Y. Yamasaki, T. Shimokawatoko, *(Osaka Gas CO., LTD.),* K. Shinkai, *(KOBE STEEL, LTD.),* S. Egashira and K. Konishi, *(KOBELCO RESEARCH INSTITUTE, INC.),* Development and Practical Application of A High Performance Open-rack LNG Vaporizer (SUPER-ORV).

[7] K. S. Lee and W. S. Kim, The Effects of Design and Operating Factors on The Frost Growth and Thermal Performance of A Flat Plate Fin-tube Heat Exchanger Under The Frosting Condition, *KSME International Journal,* 13, No. 12 (1999) 973-981.

[8] B. T. F. Chung, Z. Ma and F. Liu, General Solutions for Optimum Dimensions of Convective Longitudinal Fins with Base Wall Thermal Resistances, *Heat Transfer 1998, Proceedings of 11th IHTC,* 5 (1998), August 23-28, Gyeong-ju, Korea.

[9] D. K. Yang and K. S. Lee, Simon Song, Fin Spacing Optimization of A Fin-tube Heat Exchanger under Frosting Conditions, *Int. J. of Heat and Mass Transfer 49* (2006) 2619-2625.

[10] D. Seker, H. Karatas and N. Egrican, Frost Formation on fin-and-tube Heat Exchangers. Part I - Modeling of Frost Formation on Fin-and-tube Heat Exchangers, *Int. J. of Refrigeration 27* (2004) 367-374.

[11] D. Seker, H. Karatas and N. Egrican, Frost Formation on fin-and-tube Heat Exchangers. Part II - Experimental investigation of frost formation on fin-and-tube heat exchangers*, Int. J. of Refrigeration 27* (2004) 375-377.

[12] S. Kakac and Y. Yener, Convective Heat Transfer, *2nd edition, CRC Press* (1995) 304.

[13] K. Dhinsa, C. Bailey and K. Pericleous, Low Reynolds Number Turbulence Models for Accurate Thermal Simulations of Electronic, *5th Int. Conf. of Thermal and Mechanical Simulation and Experiments in Micro-electronics and Micro-systems,* EuroSimE2004 (2004).

[14] T. Norton, Sun Da-Wen, J. Grant, R. Fallon and V. Dodd, Applications of Computational Fluid Dynamics (CFD) in The Modelling and Design of

Ventilation Systems in The Agricultural Industry: A Review, *Int. J. of Bioresource Technology 98,* (2007) 2386-2414.
[15] Star-CD, V3.24, Methodology, *CD adapco Group* (2004) 6-1, 6-9.
[16] *NIST on-line Thermophysical Properties of Fluid System* (http://webbook.nist.gov/chemistry/fluid/).
[17] S. Kakac and Y. Yener, Convective Heat Transfer, *2nd edition, CRC Press* (1995) 301.
[18] F. P. Incropera and D. P. Dewit, Fundamentals of Heat and Mass Transfer, *4th edition, John Wiley and Sons, Inc.* (1996) 113-118.

Hyomin Jeong is currently a professor of Mechanical and Precision Engineering at Gyeongsang Nation University. He received his ph.D. in mechanical engineering from the University of Tokyo in 1992 and he joined Arizona State University as a visiting professor from 2008 to 2009. His research interests are in fluid engineering, CFD, cryogenic system, cascade refrigeration system and ejector system, mechanical vapor compression

Hanshik Chung is a professor of Mechanical and Precision Engineering at Gyeongsang National University. He obtianed his Ph.D. in Mechanical Engineering from Donga University. He joined Changwon Master's College and Tongyeong Fisher National College as an assistant Professor in 1988 and 1993, respectively. His research fields extend into the thermal engineering, heat transfer, solar heating & cooling system, LNG vaporizer optimum, solar cell, hydrogen compressor for fuel cell and making fresh water system from sea water